Applied Catalysis B: Environmental 236 (2018) 171–175

Contents lists available at ScienceDirect

Applied Catalysis B: Environmental

journal homepage: www.elsevier.com/locate/apcatb

Perspective intermediate temperature ceria based catalysts for CO oxidation

Igor V. Zagaynov[a,*], Alexander V. Naumkin[b], Yuriy V. Grigoriev[c,d]

[a] Baikov Institute of Metallurgy and Materials Science, Moscow, Russia
[b] Nesmeyanov Institute of Organoelement Compounds, Moscow, Russia
[c] Shubnikov Institute of Crystallography, Moscow, Russia
[d] NRC Kurchatov Institute, Moscow, Russia

ARTICLE INFO

Keywords:
Ceria
Solid solution
CO oxidation

ABSTRACT

The work is focused on the investigation of the influence of ternary metal oxide promoted ceria based materials (Cu-Mn-Zr-Ce-O) with various Cu/Mn molar ratios on the physicochemical and catalytic properties for CO oxidation in model reaction. It is shown that no diffraction peaks corresponding to coper and/or manganese oxides were indicated, ensuring the formation of solid solution based on ceria. The crystallite size of all samples is about 7–9 nm, and did not depend on the Cu/Mn ratio. The optimum catalyst composition was $Cu_{0.08}Mn_{0.02}(Zr_{0.1})Ce_{0.9}O_2$. To understand the feature of this optimum catalyst composition the investigation of structure and morphological characterization by XRD, TEM, HR TEM, TG-DSC, FTIR, Raman, and XPS of samples was carried out.

1. Introduction

Materials based on ceria are of interest because of they have a large oxygen storage capacity (OSC) and high mobility of oxygen, which can offer high catalytic activity and electrical conductivity. Thus, the crystal structure with a sufficiently high oxygen vacancy defect concentration is required for the effective implementation of the process. The reason is the oxygen donation of ceria caused by partial Ce^{4+}/Ce^{3+} reduction. However, the practical application of pure CeO_2 is highly discouraged due to its poor catalytic activity, thermal stability, and low surface area. In order to overcome these drawbacks, the presence of transition metals in the ceria lattice can improve these mentioned factors [1–3]. When dopants with similar or smaller radii are incorporated into ceria lattice oxygen vacancies increase, giving enhanced catalytic activity.

Manganese and copper are considered highly active and promising dopants for these goals as simple and low-cost components [4–6]. It is well known that the copper or manganese doping leads to a synergistic effect – a decrease of catalytic reaction temperature and a reduce of the activation energy, but, unfortunately, the solid solutions Cu-Mn-(Zr)-Ce-O could not be presented earlier. For example, copper or manganese is deposited by impregnation method, resulting in CuO_x-CeO_2 or MnO_x-CeO_2, respectively, but no uniform solid solution was obtained, and an additional phase was presented [4,7–9]. In some works the authors attempted to get solid solutions Cu-Mn-Ce-O (Cu/Mn = 1, Cu + Mn/Ce = 3:17; 3:7; 4:6) by the hydrothermal method [5]. Therefore, these systems can be considered highly active and promising catalysts for oxidation reactions (VOC, TWC, WGS, CO, et al.). Among them total CO oxidation and preferential CO oxidation have received more attention due to their applications in emission control and fuel cell technologies.

Structural and redox properties of catalysts are always important reason for catalytic reactions. In this work, Cu-Mn-Zr-Ce-O oxide catalysts were successfully synthesized by co-precipitation method with various Cu/Mn molar ratios, characterized by complex methods, and tested in CO oxidation reaction. The relationship between physicochemical properties of mesoporous metal oxides and their catalytic performances was discussed.

2. Material and methods

$Ce(NO_3)_3{\cdot}6H_2O$, $ZrO(NO_3)_2{\cdot}7H_2O$, $Cu(NO_3)_2{\cdot}3H_2O$, $Mn(NO_3)_2{\cdot}4H_2O$ (Acros Organics) were used as initial salts. Appropriate amounts of salts were dissolved in concentrated nitric acid (68%) with the concentration of salts of 0.667 M. After dissolution of salts, this mixture was added to distillate water, giving concentration of 0.1 M. Then, the co-precipitation was carried out by the addition of 2.5 M KOH solution up to pH 11. Ultrasonic processing (35 kHz, 150 W) was used during all process at 30 °C under stirring. The resulting precipitates were filtered, washed with distilled water-ethanol solution (H_2O/C_2H_5OH = 9 vol.), dried at 150 °C for 12 h, and calcined in static air by heating at a rate of 4 °C/min from room temperature to 500 °C and kept at 500 °C for 1 h in the muffle furnace.

All powders were characterized by XRD (DRON-3 M, Cu*Kα*

* Corresponding author.
E-mail address: igorscience@gmail.com (I.V. Zagaynov).

https://doi.org/10.1016/j.apcatb.2018.05.027
Received 6 March 2018; Received in revised form 23 April 2018; Accepted 8 May 2018
Available online 09 May 2018
0926-3373/

radiation), nitrogen adsorption-desorption method (TriStar 3000 Micromeritics), TEM (Omega Leo-912AB), HR TEM (FEI Osiris) TG-DSC (Netzsch STA449 F3), FTIR (Nicolet AVATAR330), Raman spectroscopy (HORIBA Jobin Yvon S-300).

The XPS spectra were measured on an Axis Ultra DLD spectrometer (Kratos Analytical) using a monochromatic AlK_a source (1486.6 eV, 150 W). The spectrometer was operated in fixed analysis energy mode, with a pass energy of 20 eV for high resolution spectra and 160 eV for survey spectra. The photoelectron spectra were recorded with a step of 0.1 eV. The energy scale of spectrometer was calibrated according to the standard procedure with respect to Au $4f_{7/2}$, Ag $3d_{5/2}$, and Cu $2p_{3/2}$ photoelectron peaks of pure metals at 83.96, 368.21 and 932.62 eV, respectively. The surface charging effect in the spectra was compensated against the C–H states in the C 1s spectra with the energy assumed to be 285.0 eV. The measurements were carried out at a pressure of 10^{-7} Pa at room temperature. Quantitative surface chemical analyses were calculated from the high-resolution core-level spectra, following the removal of a non-linear Shirley background.

The catalytic activity of the synthesized samples in the oxidation of CO was determined by the flow method at atmospheric pressure. The process was conducted in a U-shaped quartz reactor at the total flow rate of 60 ml/min within a temperature range of 20–500 °C. The temperature was measured with a thermocouple placed in the center of the catalytic bed. The catalyst sample mass was 0.3 g. The model gas mixture has the following composition, vol.%: CO – 1; O_2 – 2; N_2 – balance. The concentrations of gases were determined by a gas chromatograph (Varian 450GC).

3. Results and discussion

The catalytic activity of nanopowders was determined in the model oxidation reaction of CO. The conversion of carbon monoxide increases with the increase in temperature, and the curves have S-shaped type (Fig. 1). Among them, the sample 5 ($Cu_{0.08}Mn_{0.02}Ce_{0.9}O_2$, the sample numbers correspond to Table 1) has the lowest oxidation temperature. The systems with the addition of zirconium had a conversion temperature higher by 100 °C; also, the content of copper increases, the temperature decreases. The addition of zirconium is known to be always a high-temperature stabilizer of ceria lattice (T > 800 °C), that it also happens. At high operating temperatures of the catalysts this Zr dopant will manifest itself, and such catalysts will be more stable; as well as the addition of zirconium reduces the proportion of more active copper and manganese on the surface, which also explains the decrease in the activity of such systems. Therefore, the optimum catalyst composition was $Cu_{0.08}Mn_{0.02}(Zr_{0.1})Ce_{0.9}O_2$. When comparing the best catalyst with other systems based on ceria [10,11] under close test conditions, the catalytic activity of the developed catalysts was higher (the temperature of complete oxidation of CO is lower by 50–100 °C). To understand the feature of this optimum catalyst composition the other investigations of samples were carried out.

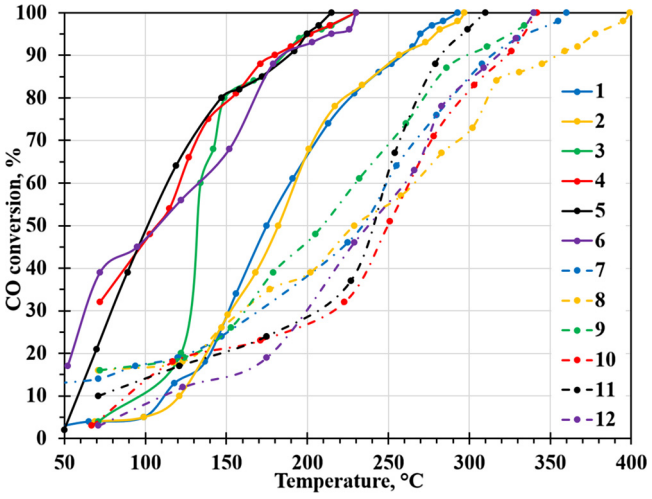

Fig. 1. Catalytic activity of samples in CO oxidation.

Table 1
Main characteristics of ceria-based powders $Cu_xMn_{0.1-x}(Zr_{0.1})Ce_{0.8}O_2$.

No	Sample	d_{XRD}, nm	S_{BET}, m^2/g	Cumulative volume of pores, cm^3/g
0	CeO_2 [12]	14	53	0.1070
1	$Cu_0Mn_{0.1}Ce_{0.9}O_2$	9	91	0.3185
2	$Cu_{0.02}Mn_{0.08}Ce_{0.9}O_2$	7	84	0.2469
3	$Cu_{0.04}Mn_{0.06}Ce_{0.9}O_2$	7	91	0.2837
4	$Cu_{0.06}Mn_{0.04}Ce_{0.9}O_2$	8	94	0.2532
5	$Cu_{0.08}Mn_{0.02}Ce_{0.9}O_2$	9	79	0.2127
6	$Cu_{0.1}Mn_0Ce_{0.9}O_2$	12	55	0.1858
7	$Cu_0Mn_{0.1}Zr_{0.1}Ce_{0.8}O_2$	7	75	0.3291
8	$Cu_{0.02}Mn_{0.08}Zr_{0.1}Ce_{0.8}O_2$	6	67	0.1863
9	$Cu_{0.04}Mn_{0.06}Zr_{0.1}Ce_{0.8}O_2$	7	71	0.2501
10	$Cu_{0.06}Mn_{0.04}Zr_{0.1}Ce_{0.8}O_2$	7	36	0.1140
11	$Cu_{0.08}Mn_{0.02}Zr_{0.1}Ce_{0.8}O_2$	8	31	0.0868
12	$Cu_{0.1}Mn_0Zr_{0.1}Ce_{0.8}O_2$	8	40	0.1159

The XRD patterns of the samples are shown in Fig. 2. All samples present the characteristic peaks of pure cubic fluorite structure of ceria, and other phases (MnO_x, CuO_x, $CuMnO_x$) were not detected, indicating the fine dispersion of dopants and the solid solution formation. It is know that the solubility limit for Mn and Cu in ceria is less than 20–30 and 5-10 mol.%, accordingly, and highly depends on the preparation method [13,14]. The crystallite size of solid solutions is presented in Table 1. The crystallite size of all samples is about 7–9 nm, and do not depend on the Cu/Mn ratio. According to TEM, all powders consisted of particle aggregates (Fig. 3); individual near-spherical nanoparticles were about 4–10 nm, which corresponds to the crystallite size, calculated by Scherrer equation. Doping in a ceria lattice induces uniform strain in the lattice because the material is elastically deformed. This effect causes the lattice plane spacing to change and the diffraction peaks to shift to new 2θ positions [15]. Nevertheless, it is known that the preparing of homogeneous solid solutions gives the better textural property, thermal stability, catalytic properties and others compared to domain- or phase-segregated nonhomogeneous ones. SAED method (Fig. 3) also confirmed the formation of the only phase – fluorite structure solid solution. According to TG-DSC, these solid solutions are stable up to 1400 °C.

Fig. 4 shows the Raman spectra of the materials. In contrast to XRD

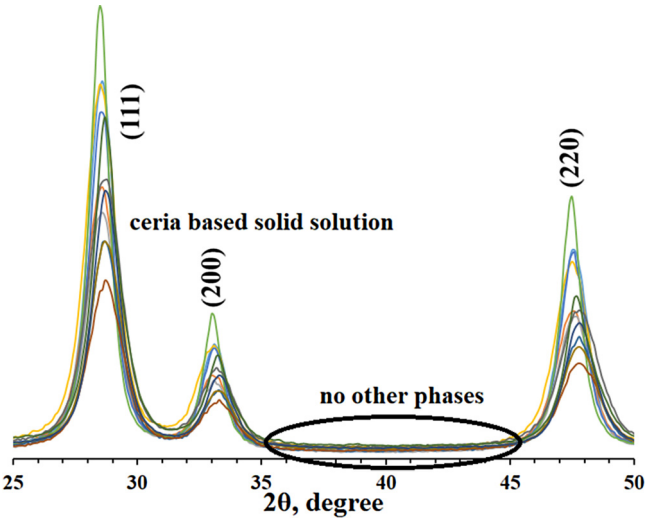

Fig. 2. XRD patterns of calcined powders.

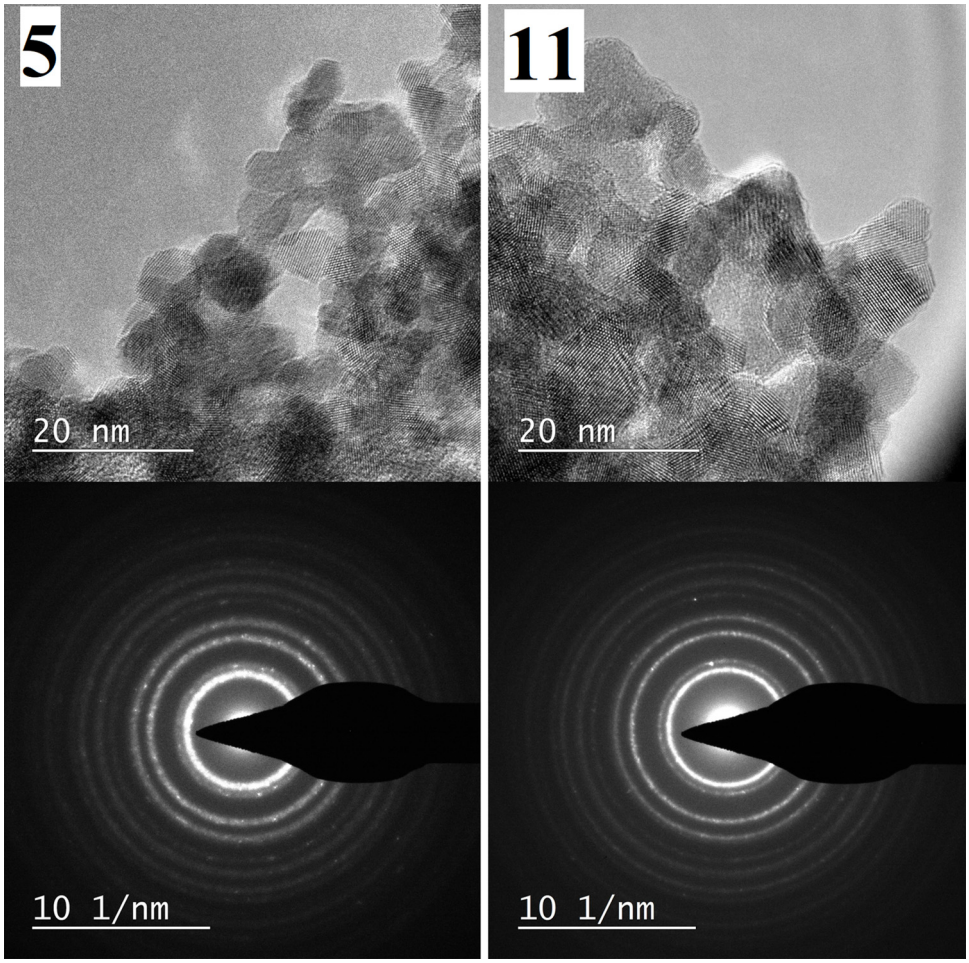

Fig. 3. HR TEM microphotos of powders of samples 5 and 11.

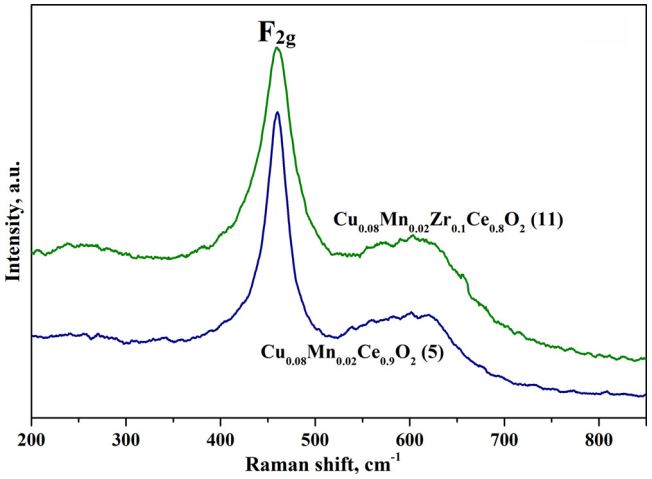

Fig. 4. Raman patterns of catalysts 5 and 11.

results, which afford information, related to the cation sublattice, Raman spectroscopy of the catalysts is dominated by oxygen lattice vibrations. The strong band at 460 cm^{-1} is attributed to the F_{2g} Raman vibration mode of the cubic fluorite structure phase, which also suggests that dopant ions (copper, manganese, zirconium) have been incorporated into the ceria lattice to form solid solutions, and the broad band at 590 cm^{-1} is attributed to the oxygen vacancies generated by the partial substitution of dopant ions to Ce^{4+}. The relative concentration of oxygen vacancies in the solid solutions can be represented by the area ratio of peaks 590 and 460 cm^{-1}, and the results suggest that the incorporation of these dopants into the ceria lattice increases the concentration of oxygen vacancies. The greater number of oxygen defects may account for the improved oxygen storage capacity, and enhance CO oxidation activity [5,16].

All samples have IV type adsorption curves with a hysteresis loop (not shown) indicating the presence of mesopores in the systems [15]. There was the increase of a specific surface (Table 1) with increasing content of manganese or the decrease with adding zirconium. Polymodal pore size distributions were observed in the range of 2–25 nm for Cu-Mn-Ce-O systems and 2-40 nm for Cu-Mn-Zr-Ce-O. No micropores (< 2 nm, according to t-plot method) were observed in all samples, and no regularity in the change of Cu/Mn ratio was too.

XPS analysis was used to investigate the surface of the best catalysts (samples 5 and 11) before and after catalytic test. Fig. 5 shows spectra of O 1s, taking into account surface charge for which was carried out for the state C—C/C—H, isolated in the spectrum of C 1s (not shown), and over the peak u"' in the spectrum of Ce 3d, to which the energies of 285 and 916.4 eV were assigned, respectively. It is seen that in the first case the spectrum of sample 11 is shifted towards lower binding energies by ~ 0.4 eV, and in the second case, the spectra basically coincide, excluding the region of about 531 eV. It follows that adventitious carbon interacts with the carrier in various ways, which should also be taken into account in catalytic processes, but it is seen that there is no change in the spectrum after catalysis (samples 5 before and after). By using the curve-fitting approach, this spectrum can be divided into three components: lattice oxygen (528–530 eV), surface oxygen (530–532 eV), and adsorbed oxygen species (532–534 eV) from hydroxyl species and

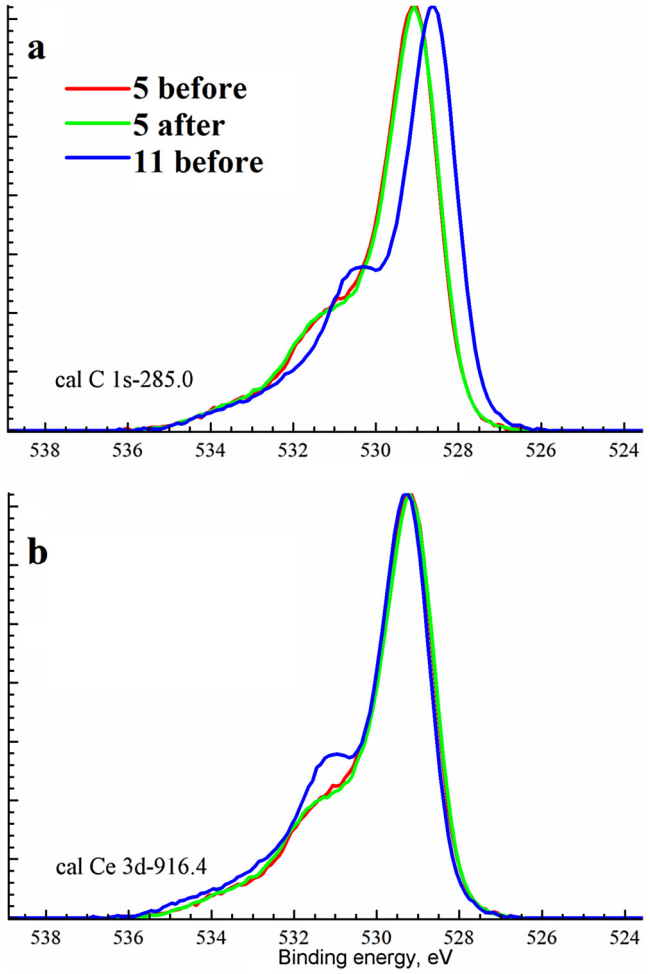

Fig. 5. X-ray photoelectron spectra of O 1s of the catalysts before and after reaction, normalized to the intensity of the main peak and calibrated for the peaks C 1s (a) and Ce 3d (b).

adsorbed water [17]. With the addition of dopants, the binding energy of O 1 s of lattice oxygen shifts to higher values due to oxygen-metal electron-transfer process, and this can create very active electrophilic oxygen species. It is known that O^-, O_2^-, O_2^{2-} species are very active for the oxidation process. Therefore, a higher concentration of surface oxygen would be beneficial for enhancing the catalytic activity.

All spectra of Ce 3d indicate the presence of only the Ce^{4+} state (Fig. 6). This conclusion is based on the energy position of the photoelectron peaks and their relative intensities. Minor differences in the spectra of samples are associated with their different resistance to X-ray radiation during the recording of spectra. This was illustrated by the spectra measured at the beginning of the experiment and at the end (not shown). It should be noted that the spectra of sample 11 practically coincide. Perhaps this is due to the large ratio of concentrations of Mn/Ce and the fact that Mn increases the radiation resistance of CeO_2. Earlier it was shown that for the spectra of Mn-Ce-O samples the ratio of the peaks u'''/v is close to one, because for samples based on pure ceria it is noticeably less than one. This is also supported by the analysis of many published data.

During the survey of the spectra, a partial decomposition of sample 5 took place, while the spectrum of sample 11 remained unchanged. Proceeding from this, it is possible to draw a conclusion about the appearance of the Ce^{3+} state during the survey, but it cannot be asserted that it was in the beginning. If it is assumed that the spectrum of sample 11 reflects only the state of Ce^{4+}, then one can estimate the fraction of the Ce^{3+} state by subtracting it from the spectra of samples 5 before

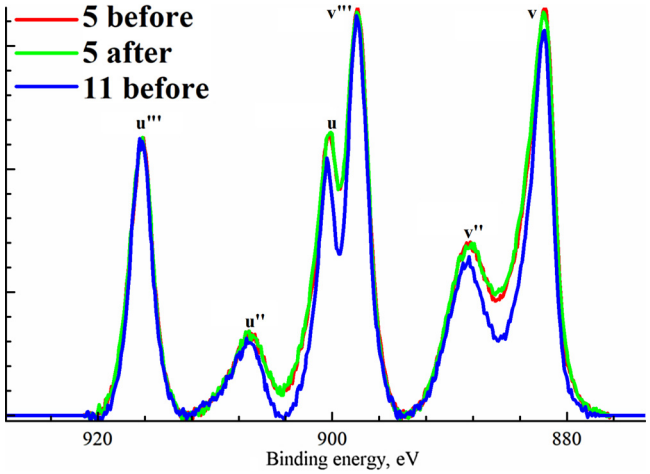

Fig. 6. Comparison of the Ce 3d spectra of samples 5 and 11. The spectra are normalized by the intensity of the peak u'''.

and after, but the question of the presence of the Ce^{3+} state in sample 11 remains open. In this case, the relative content of Ce^{3+} state is about 16% and 17% before and after catalytic test, respectively. In previous works the same relative content of Ce^{3+} state was estimated [18], but in another work this value was obviously overestimated (relative content of Ce^{3+} was 20–34%) [6].

In all spectra of Cu 2p and Mn 2p present states: Cu^+ and Cu^{2+}, Mn^{2+}, Mn^{3+}, and Mn^{4+} (Fig. 7). The mole portion of Cu is calculated on the basis of the analysis of the relative intensity of the satellite and

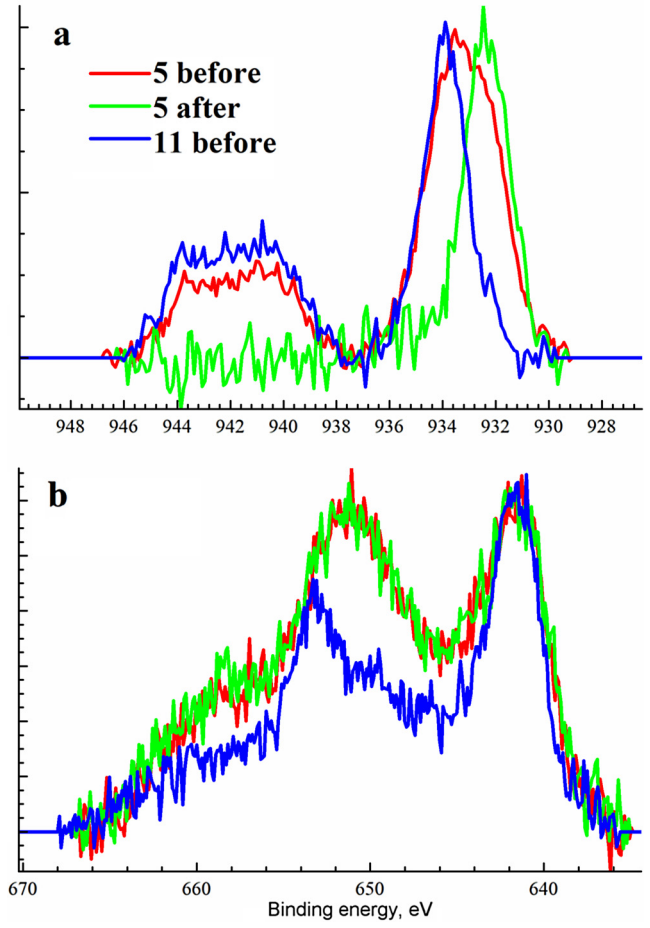

Fig. 7. X-ray photoelectron spectra of Cu 2p (a) and Mn 2p (b).

Table 2
The surface composition (XPS) of catalysts before and after catalytic test.

No	Sample	Cu/Mn/(Zr)/Ce (synthesis)	Cu/Mn/(Zr)/Ce (XPS)	Cu ratio (%)		Mn ratio (%)		
				Cu^{+}	Cu^{2+}	Mn^{2+}	Mn^{3+}	Mn^{4+}
5 before	$Cu_{0.08}Mn_{0.02}Ce_{0.9}O_2$	4/1/0/45	3.1/1/0/27.4	38	62	24	49	27
5 after	$Cu_{0.08}Mn_{0.02}Ce_{0.9}O_2$	4/1/0/45	3.0/1/0/27.2	33	67	22	54	24
11 before	$Cu_{0.08}Mn_{0.02}Zr_{0.1}Ce_{0.8}O_2$	4/1/5/40	1.5/1/3.1/16.6	5	95	22	65	13

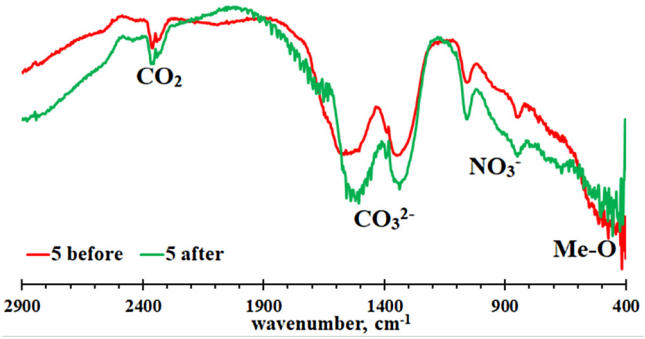

Fig. 8. FTIR spectra of sample 5 before and after catalysis.

the position of the Auger peak. The results are presented in Table 2. The real ratio of Cu to Mn on the surface is lower than theoretical ratio in sample 5 (before and after) and especially in sample 11. Therefore, it means that the surface is enriched with manganese, and copper enters inward the crystalline structure of the particle, especially, in the presence of zirconium, which apparently displaces it with no significant changes before and after catalysis. There is also a significant decrease in the fraction of Cu^{+} in the presence of Zr, as well as an increase in the intermediate Mn^{3+}, and after the catalytic test, the proportion of this manganese also increases. Thus, it can be assumed that the copper with low oxidation state (Cu^{+}) is easily oxidized; and the manganese species with low oxidation state (Mn^{2+}) are oxidized and with high oxidation state (Mn^{4+}) are easily reduced to intermediate state Mn^{3+}. Oxide catalyst possessing numerous oxidation states to facilitate electron transfer processes can be efficient catalysts for CO oxidation; this phenomenon can be explained by synergistic interaction in solid solution, and can be conducive to form more surface oxygen vacancies:

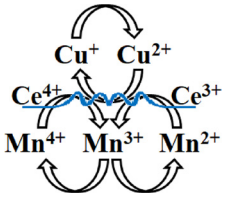

FTIR spectra show Me—O band at 400–500 cm^{-1} attributed to the vibration of ceria-based solid solution. Samples also have residual nitrate and carbonate groups; as seen there are no changes in the spectra before and after catalysis in sample 5 (Fig. 8).

4. Conclusions

In this study Cu-Mn-Zr-Ce-O solid solutions with the crystallite size about 7–9 nm, not depending on the Cu/Mn ratio, were prepared via the co-precipitation method with sonication. The full conversion of CO can reach at 200-300 °C for Cu-Mn-Ce-O systems and at 300–400 °C for Cu-Mn-Zr-Ce-O systems, and the optimum catalyst composition was $Cu_{0.08}Mn_{0.02}Ce_{0.9}O_2$ with temperature of 215 °C and $Cu_{0.08}Mn_{0.02}Zr_{0.1}Ce_{0.9}O_2$ with temperature of 310 °C. The formation of these stable solid solutions by doping copper and manganese enhances the redox properties, oxygen vacancies, stability, and, of course, catalytic activity. These systems can be used in catalysis both by themselves and as supports.

Acknowledgments

This research was supported by Russian Science Foundation (No. 17-73-10331). This work was partially conducted within the framework of budget project No. 007-00129-18-00 (XRD and FTIR investigations).

References

[1] A. Trovarelli, Catalysis by Ceria and Related Materials, World Scientific Publishing Company, Singapore, 2002.
[2] A. Trovarelli, P. Fornasiero, Catalysis by Ceria and Related Materials, 2nd ed., World Scientific Publishing Company, Singapore, 2013.
[3] A. Trovarelli, Structural and oxygen storage/release properties of CeO_2-based solid solutions, Comments Inorg. Chem. 20 (1999) 263–284.
[4] H. Lu, X. Kong, H. Huang, Y. Zhou, Y. Chen, Cu–Mn–Ce ternary mixed-oxide catalysts for catalytic combustion of toluene, J. Environ. Sci. 32 (2015) 102–107.
[5] C. Li, Z. Li, H.Y. Oh, G.H. Hong, J.S. Park, J.M. Kim, Ordered mesoporous Cu-Mn-Ce ternary metal oxide catalysts for low temperature water-gas shift reaction, Catal. Today 307 (2018) 237–242.
[6] C. He, Y. Yu, J. Shi, Q. Shen, J. Chen, H. Liu, Mesostructured Cu–Mn–Ce–O composites with homogeneous bulk composition for chlorobenzene removal: catalytic performance and microactivation course, Mater. Chem. Phys. 157 (2015) 87–100.
[7] Q. Liang, X. Wu, D. Weng, H. Xu, Oxygen activation on Cu/Mn–Ce mixed oxides and the role in diesel soot oxidation, Catal. Today 139 (2008) 113–118.
[8] X. Zhou, M. Meng, Z. Sun, Q. Li, Z. Jiang, Prominent enhancement of Mn or Co addition on the performance of Cu-Ce-O catalyst used for H_2 production via dimethyl ether steam reforming, Chem. Eng. J. 174 (2011) 400–407.
[9] H. Lu, Y. Zhou, H. Huang, B. Zhang, Y. Chen, In-situ synthesis of monolithic Cu-Mn-Ce/cordierite catalysts towards VOCs combustion, J. Rare Earth 29 (2011) 855–860.
[10] D. Mukherjee, B.G. Rao, B.M. Reddy, CO and soot oxidation activity of doped ceria: influence of dopants, Appl. Catal. B 197 (2016) 105–115.
[11] D. Devaiah, T. Tsuzuki, C.U. Aniz, B.M. Reddy, Enhanced CO and soot oxidation activity over Y-doped ceria–zirconia and ceria–lanthana solid solutions, Catal. Lett. 145 (2015) 1206–1216.
[12] I.V. Zagaynov, A.V. Vorobiev, S.V. Kutsev, Synthesis of mesoporous ceria-based nanopowders for functional materials application, Mater. Lett. 139 (2015) 237–240.
[13] A. Aranda, E. Aylón, B. Solsona, R. Murillo, A.M. Mastral, D.R. Sellick, S. Agouram, T. García, S.H. Taylor, High activity mesoporous copper doped cerium oxide catalysts for the total oxidation of polyaromatic hydrocarbon pollutants, Chem. Comm. 48 (2012) 4704–4706.
[14] Ch.Y. Kang, H. Kusaba, H. Yahiro, K. Sasaki, Y. Teraoka, Preparation, characterization and electrical property of Mn-doped ceria-based oxides, Solid State Ion. 177 (2006) 1799–1802.
[15] I.V. Zagaynov, A.A. Konovalov, E.A. Koneva, Investigation of structure and morphology of Cu-Mn-Zr-Ce-O solid solutions, Lett. Mater. 8 (2018) 135–139.
[16] W.Y. Hernandez, M.A. Centeno, F. Romero-Sarria, J.A. Odriozola, Synthesis and characterization of $Ce_{1-x}Eu_xO_{2-x/2}$ mixed oxides and their catalytic activities for CO oxidation, J. Phys. Chem. C 113 (2009) 5629–5635.
[17] X.F. Tang, Y.G. Li, X.M. Huang, Y.D. Xu, H.Q. Zhu, et al., MnO_x–CeO_2 mixed oxide catalysts for complete oxidation of formaldehyde: effect of preparation method and calcination temperature, Appl. Catal. B 62 (2006) 265–273.
[18] C. Deng, Q. Huang, X. Zhu, Q. Hu, W. Su, et al., The influence of Mn-doped CeO_2 on the activity of CuO/CeO_2 in CO oxidation and NO + CO model reaction, Appl. Surf. Sci. 389 (2016) 1033–1049.